Available online at www.sciencedirect.com
ScienceDirect
Journal of the European Ceramic Society 28 (2008) 2129–2135
www.elsevier.com/locate/jeurceramsoc

High temperature characterisation of cordierite–mullite refractory by ultrasonic means

T. Chotard [a,*], J. Soro [a], H. Lemercier [b], M. Huger [a,*], C. Gault [a]

[a] *Groupe d'Etude des Matériaux Hétérogènes (GEMH, EA 3178), Ecole Nationale Supérieure de Céramique Industrielle, 47 à 73 Avenue Albert Thomas, 87065 Limoges Cedex, France*
[b] *Terreal-CRED, Route de Revel, 11400 Castelnaudary, France*

Received 26 November 2007; received in revised form 15 February 2008; accepted 29 February 2008
Available online 2 May 2008

Abstract

Refractory materials containing cordierite ($2MgO{\cdot}2Al_2O_3{\cdot}5SiO_2$) and mullite ($3Al_2O_3{\cdot}2SiO_2$) are used as support in furnaces, because of their low thermal expansion properties (coefficient of thermal expansion (CTE) ≈ 3–$4 \times 10^{-6}\,K^{-1}$) which confer them a very good ability to thermal shock resistance. Composed of two phases presenting very different CTE (1.5–3×10^{-6} for cordierite and 4–$6 \times 10^{-6}\,K^{-1}$ for mullite), these materials can develop damage during thermal cycling due to internal stresses. This paper is devoted to the characterisation of the damage generated by this CTE mismatch, thanks to the application of ultrasonic techniques like long bar mode echography and acoustic emission (AE). The combination of these two techniques allows, during the applied thermal cycle (20–1200 °C), to continuously follow both the evolution of the elastic properties (Young's modulus) and the acoustic emission activity generated within the material. The analysis of these two characteristics, which are closely related to the damage evolution, makes it possible to propose a chronology of the mechanisms (damage, expansion) acting during the heating and the cooling stages.

Keywords: Non-destructive evaluation; Thermal expansion; Mechanical properties; MgO–Al_2O_3–SiO_2; Refractories

1. Introduction

The heterogeneity of industrial refractory materials results from their multiphase composition involving aggregates of different sizes, bonding phases and various additives. The grains arrangement, the shape of aggregates and the microstructural defects such as porosity and cracks, make difficult the prediction of the mechanical and thermal behaviours.

The understanding of the thermomechanical behaviour of refractory materials is essential for their use as linings in high temperature furnaces and refining vessels in the metallurgical, cement, and petrochemical industries. The increasing application of the finite element calculations for the prediction of the behaviour in real conditions requires the knowledge of mechanical properties closely related to damage evolution at high temperature which corresponds to the domain of use of these materials.

Cordierite–mullite refractory materials are very widely used in ceramic industry as support parts in furnace. Considering their service conditions, they are subjected to repeated thermal cycles. These materials have a complex microstructure characterised by crystalline phases presenting both thermal expansion mismatches and different elastic properties, and by a residual silicate glassy phase. There exist, as in many multiphase refractories, some microstructural phenomena acting throughout the thermal cycles and inducing internal stresses as well as damage during cooling which are mainly due to the existence of disagreements in thermal expansion properties.[1,2] In this study, the evolution of the material at high temperature, and specifically its damage, is monitored during specific thermal cycles by two complementary non-destructive acoustic methods: an ultrasonic pulse echography (US Echo) in long bar mode allows the calculation of Young's modulus and the acoustic emission technique (AE) is applied to follow the evolution of damage within the material at a very local scale.

* Corresponding authors.
E-mail addresses: t_chotard@ensci.fr (T. Chotard), m_huger@ensci.fr (M. Huger).

0955-2219/$ – see front matter © 2008 Elsevier Ltd. All rights reserved.
doi:10.1016/j.jeurceramsoc.2008.02.029

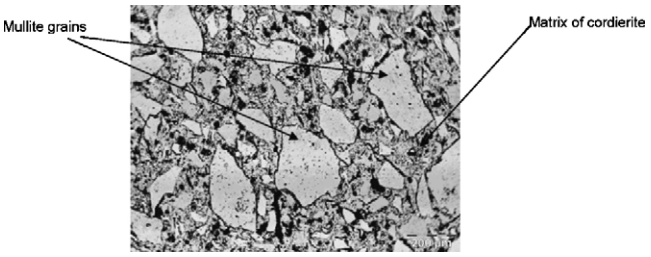

Fig. 1. Typical micrography of cordierite–mullite refractory.

Classically, AE technique is applied to characterise the damage of structures such as pressure tanks, carrying structures, and so on. Its use can also be helpful to better understand and to identify the damage mechanisms occurring in the materials subjected to mechanical loading.[3–6] Recently, this technique has been adapted for the characterisation of cement setting and to detect the emptying of capillary networks in a porous material during drying.[7,8] The originality of this work resides in the coupled application, on a refractory material subjected to thermal cycling at high temperature, of both AE technique to characterise and to identify the damage phenomena, and also of the ultrasonic echography in order to better understand the effect of damage process on the evolution of elastic properties.

2. Materials and methods

2.1. Materials

The tests were carried out on a cordierite–mullite refractory material industrially used like support in furnace for roof tiles and bricks manufacture. It is a two-phase refractory (Fig. 1) constituted of mullite grains (Al_2O_3–$2SiO_2$) in a matrix of cordierite ($2MgO$–$2Al_2O_3$–$5SiO_2$). For this commercial material, the exact proportions of each component were not communicated. However, the results of previous analyses make it possible to have an idea of the composition (cordierite: 70 wt%/mullite: 30 wt%). Having very low thermal expansion properties ($CTE_{average}$ ranging from 1.5 to $3 \times 10^{-6}\,K^{-1}$), cordierite has an excellent thermal shocks resistance. However, at high temperature (starting from 1200 °C), the creep resistance of cordierite is poor. Mullite, which has a good mechanical resistance at high temperatures and can be elaborated from low cost raw materials, is usually added as a second phase to balance this weakness. Indeed, mullite is an alumino-silicate which can be obtained by various ways, phase transformation of andalusite or by decomposition of kaolinite according to the following equations:

$$\underset{\text{andalusite}}{3(Al_2O_3\text{–}SiO_2)} \rightarrow \underset{\text{mullite}}{3Al_2O_3\text{–}2SiO_2} + SiO_2 \quad (1)$$

$$\underset{\text{kaolinite}}{3(Al_2O_3\text{–}2SiO_2\text{–}2H_2O)} \rightarrow \underset{\text{mullite}}{3Al_2O_3\text{–}2SiO_2} + 4SiO_2 + 6H_2O \quad (2)$$

These reactions involve a residual silicate phase and can lead to the creation of different secondary phases within the same grain due to impurities. Mullite has a rather high thermal expansion, compared to that of cordierite, leading to a significant thermal expansion mismatch with this last material (Table 1). This differential of dilation is the source of the internal stresses which appear during thermal cycles inducing a significant damage, in particular when cooling.

Table 1
Thermal and elastic properties for each component of the two-phase material

	Young's modulus (E, GPa)	Coefficient of thermal expansion, CTE (α, $10^{-6}\,K^{-1}$)
Cordierite (matrix)	132	1.4–2.6
Mullite (grains)	220	4.5–5.3

2.2. Ultrasonic pulse echography (US Echo)

The main interest of this technique is to be able to follow the evolution of the Young's modulus, which is both depending on the intrinsic elastic properties of constituents, and also related to the damage of material, according to the temperature. This measurement is made in the configuration known as of "long bar mode", i.e. that side dimensions d of the sample are small compared to the wavelength λ of the ultrasonic vibration ($d/\lambda < 0.2$). The experimental device developed in the laboratory[9,10] is presented in Fig. 2.

A transducer (frequency = 85 kHz), placed in the cold zone of the system, generates an ultrasonic pulse which is transmitted to the sample located in the furnace through an alumina wave guide. The studied sample, parallelepiped of dimension 5 mm × 4 mm × 100 mm, is stuck on the waveguide with a refractory cement. Young's modulus E is calculated by the following formula:

$$E = \rho \times \left(\frac{2L}{\tau}\right)^2 \quad (3)$$

where ρ is the density of the sample (here 2.11 g cm^{-3}), L the sample length and τ the time of flight of the wave after a round trip in the sample. This technique makes it possible to have a global idea of the microstructural and damage evolutions within

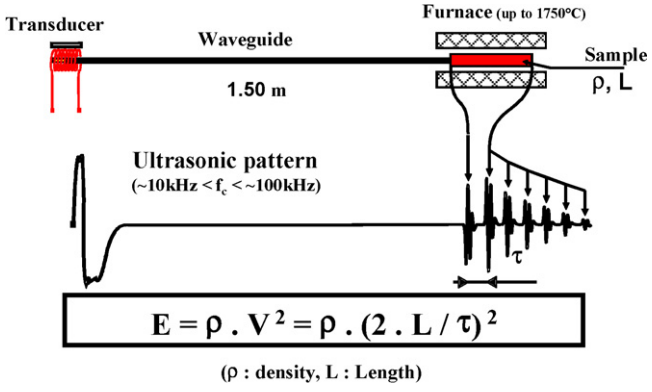

Fig. 2. Experimental setup used for Young's modulus measurement at high temperature by long bar mode pulse echography.

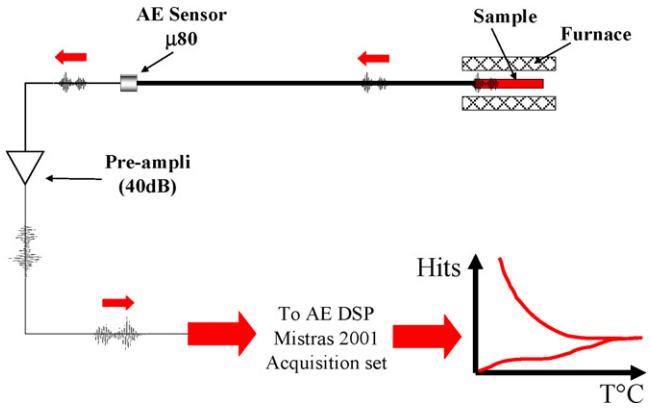

Fig. 3. Experimental setup used for high temperature acoustic emission (AE) measurements.

the material by measuring, during thermal cycles, the values of the modulus E. In particular, Young's modulus decreases when damage (microcracking) occurs in the material. On the contrary, crack healing phenomena are accompanied by an increase of Young's modulus.

2.3. Acoustic emission

AE is defined as phenomena whereby transient elastic waves are generated by the rapid release of energy from localised sources within a material (or structure). When a material is subjected to solicitations (such as mechanical, thermal, etc.), acoustic emission can be generated by a variety of sources, including crack nucleation and propagation, multiple dislocation slip, twinning, grain boundary sliding, Barkhausen effect (realignment or growth of magnetic domains), phase transformations in alloys, debonding of fibres in composite materials or fracture of inclusions in alloys.[11–17] This technique has been used either at the laboratory level or industrial scale. Usually, this technique is applied at room temperature as a non-destructive characterisation technique in order to follow in real-time the evolution of the damage of a material subjected to mechanical loading.[18–22] Here, the application of AE technique aims to characterise in situ at high temperature the damage or other microstructural transformations taking place in the material resulting from a particular thermal configuration.

The device of acquisition (Fig. 3), rather similar to that of the ultrasonic pulse echography, is composed of a wide band (175 kHz–1 MHz) sensor (PAC MICROPHONE µ80), a preamplifier (EPA 1220A) and an acquisition card associated with a computer (AEDSP-32/16 MISTRAS digital system from Physical Acoustics Corporation). The AE sensor is a major element of the chain of acquisition because it collects the whole of the signals induced by the elastic waves created within the material whose amplitudes are higher than a fixed threshold in order to amplify and to record them. This system records the waveform and the main feature parameters well known in AE study such as count, hit, rise time, duration of hit, count to peak, amplitude (in dB). Fig. 4 presents different AE features extracted from the signal waveform.

A classical analysis of the evolution of the number of cumulated hits (N) during the thermal cycle will be also carried out as well as a calculation of the hits rate according to the considered temperature:

$$R_T = \frac{d(N)}{d(T)} \quad (4)$$

With R_T in K^{-1}.

Thermal cycling is the same for both US Echo and AE testing, that means:

- Heating at 5 °C min^{-1} from room temperature up to 1215 °C.
- Dwell of 0.2 h at 1215 °C.
- Cooling at 5 °C min^{-1} down to room temperature.

The maximum temperature as well as the temperature rate were selected in order to reproduce, as precisely as possible, the operating conditions of this material.

2.4. Dilatometry measurements

Dilatometric measurements were conducted to support our investigations and to refine our interpretations. These tests were carried out on samples (at least 3) of dimension (10 mm × 5 mm × 5 mm) thanks to an ADAMEL DI24

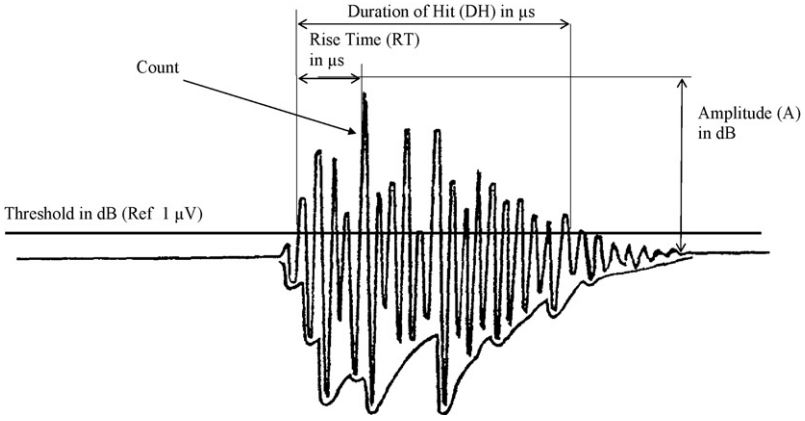

Fig. 4. Typical AE features extracted from the recorded signal (hit).

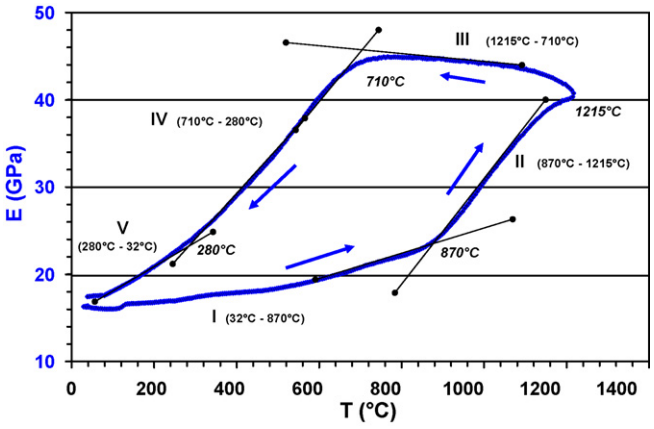

Fig. 5. Young's modulus evolution according to the temperature for a cordierite–mullite sample.

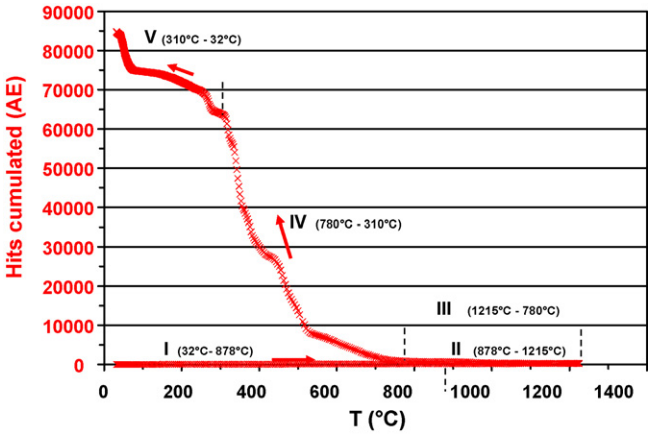

Fig. 6. Cumulated number of hits (AE) vs. temperature curve for a cordierite–mullite sample.

dilatometer. The thermal cycle carried out is the same one as previously quoted.

3. Results and discussion

3.1. High temperature ultrasonic pulse echography

Fig. 5 presents the variation of Young's modulus vs. temperature. On this figure, five characteristic periods concerning of the evolution of the elastic properties of the material can be clearly distinguished. From room temperature up to approximately 870 °C (Period I), we can quote a slight but continuous increase of the Young's modulus which goes from 16 GPa at 20 °C to around 24 GPa at 870 °C. Above this temperature, a strong inflection of E is observed up to the dwell (1215 °C) (period II). Indeed, during this heating period, the value of the Young's modulus practically doubles ($E \approx 40$ GPa) suggesting that major modifications occur within the material. Period III (1215–710 °C) corresponds to the beginning of the cooling stage. Throughout this domain of temperature, E continues to evolve to higher values until approximately 710 °C, where it reaches its maximum ($E \approx 45$ GPa). But, at the end of this stage, the Young's modulus starts to decrease significantly which is confirmed in stage IV (710–280 °C). The last period (V, from 280 °C to room temperature) is still associated to a drop of E, however less marked than for the previous temperature domain. At the end of this period, the Young's modulus reaches a value close to that it had before the thermal cycle ($E \approx 18$ GPa).

3.2. High temperature acoustic emission

Figs. 6 and 7 present the evolution of the cumulated number of AE hits (N) vs. temperature, during the same thermal cycle than the one used for ultrasonic experiment. From room temperature to 878 °C (period I), one observes a continuous increase in the number of recorded hits associated however with a rather low hit rate ($R_T = 0.18\ K^{-1}$). Period II (878 °C up to 1215 °C) presents a recrudescence of the acoustic activity (Fig. 7) with a hit rate value almost multiplied of a factor 3 (Table 2). The cooling stage of the cycle is separated into three temperature ranges. The

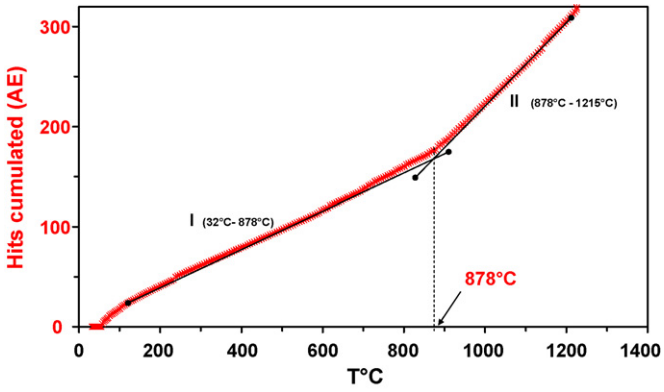

Fig. 7. Cumulated number of hits (AE) vs. temperature curve for a cordierite–mullite sample: heating periods.

beginning of cooling (period III from 1215 °C down to 780 °C) is characterised by a rather constant acoustic activity with a hit rate multiplied by 3 compared with the one of the previous period (Table 2). From 780 °C to approximately 310 °C (period IV), the acoustic emission has an exponential increase (Fig. 6) associated to a considerable rise of R_T (Table 2). Below 310 °C and down to room temperature, (period V), one observes a slight deceleration of the hit rate even if the acoustic activity (N) remains constant.

4. Discussion

It is interesting to compare the results obtained from the two acoustic non-destructives techniques (Echo US and AE) jointly applied (Fig. 8) and from dilatometry measurements in order to better understand the phenomena acting within the sample during the thermal cycles. Taking into account the carried out thermal cycles, the logic of the experimenter would like that the discussion of the results considers as the starting point the heating phase of the material. However, from a mechanical point of view, it seems more judicious to consider the beginning of cooling stage as a state free of internal stresses which are developed during the fall of temperature occurring during the elaboration of the material. For this reason, the discussion will be initially held on cooling stages, then on the heating ones. To have a more

Table 2
Summary of the AE characteristics for each temperature domain

Stage number	I	II	III	IV	V
Temperature domain	Heating from 32 °C up to 878 °C	Heating from 878 °C up to 1215 °C	Cooling from 1215 °C down to 780 °C	Cooling from 780 °C down to 310 °C	Cooling from 310 °C down to 32 °C
Cumulated hits by period (N)	150	170	653	57,484	26,417
$\lvert R_T \rvert$ K^{-1}	0.18	0.50	1.5	127	87

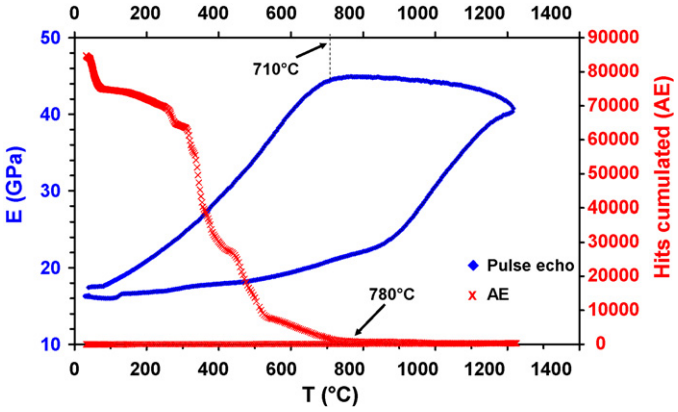

Fig. 8. Combined evolution of the modulus of elasticity and the acoustic activity (cumulated number of hits) according to the temperature for a cordierite–mullite sample.

accurate interpretation of the phenomena acting during these stages, a simple theoretical model based on a two-phase material can be considered: mullite grains inside a matrix of cordierite. According to this model, if we assume that the average coefficient of thermal expansion of the grains (α_g) ranges from 4.5 to 5.3 × 10^{-6} K^{-1} and the one for the matrix (α_m) goes from 1.4 to 2.6 × 10^{-6} K^{-1}, the thermal expansion mismatch, noted $\Delta\alpha = \alpha_m - \alpha_g$ is thus negative during thermal cycles.

Period III (*cooling from* 1215 *to* 710 °C): During this stage, the observed increase of E is due to the regular stiffening of the material when temperature decreases. In this temperature range, the material behaves like a sintered ceramic with a small amount of glassy phase. The observation of the dilatometric curve confirms this tendency. Indeed, the dilatometric behaviour of the material (Fig. 10) is very close of the one of mullite. At the beginning of this stage, the grain–matrix interface is cohesive and the coefficient of thermal expansion (CTE) is that of the undamaged material strongly influenced by that of mullite (ranging approximately from 4 to 6 × 10^{-6} K^{-1}). At the same time, the recorded AE activity confirms that this increase in rigidity is most probably associated with a phenomenon of sliding at a very local scale (micro-displacements between grains within the matrix). In fact, at the grain–matrix interface (assumed to be cohesive at the beginning of cooling), the surface of the matrix (Fig. 9) is stressed in compression circumferentially (σ_{ortho}) and radially in tension (σ_{rad}) because its shrinkage is lower than that the one of the grain ($\alpha_g > \alpha_m$). This state of stress is increasing with the decrease of temperature and induces micro-sliding of the grains (at high temperature) and probably the early onset of microcracks at the interface when reaching lower temperature (around 780 °C). However, these observations can be interpreted in a contradictory way. Indeed, how can we associate, in the last part of this temperature domain, an increase (even slight) of the elastic properties with an onset (also even slight) of damage? This phenomenon can be explained by the difference in the principle of measurement existing between the two characterisation methods. In fact, where US echography gives information on the wave velocity based on the integration of the material mechanical properties on a given volume, the AE technique, itself, is sensitive to all the events occurring in this volume. It is thus not surprising that, thanks to its great sensitivity, the AE technique can detect, in a distinct way, the occurrence of phenomena before they have an influence on the mechanical behaviour of the material, itself characterised by the US echography.

Period IV (*cooling from* 710 *to* 280 °C): while this temperature domain, a significant drop of the elastic properties of the material occurs (Fig. 5). This fall is related to development of damage induced by the thermal expansion mismatch existing between phases. The probable superimposition of onset process and propagation of microcracking is confirmed by an important rise of the hit rate (R_T = 127 K^{-1}) associated to the highest

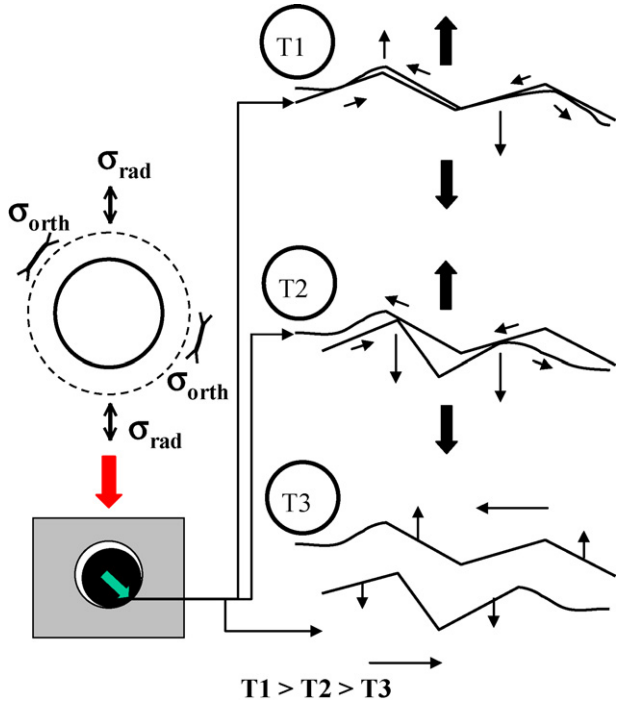

Fig. 9. Schematic representation of residual stresses developed and hypothesis on mechanisms acting during the cooling stage: (T1) tensile and shear stresses at the grain–matrix interface and early micro-displacements; (T2) displacement at interfaces and early onset of microcracking; and (T3) propagation of damage and generalised interfacial decoherence process.

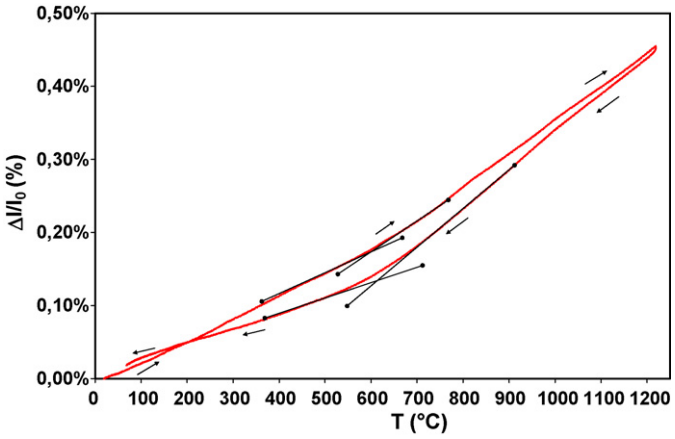

Fig. 10. Dilatometric evolution of a cordierite–mullite sample during a thermal cycle.

number of recorded hits (Table 2). Here again, the dilatometric curve (Fig. 10) comes to support our assumptions. From a specific temperature (around 600 °C), the effect of the progressive decoherence of the mullite grains causes the reduction of the global CTE of the material which tends towards that of cordierite (ranging approximately from 1.5 to $3 \times 10^{-6}\,K^{-1}$).

Period V (*cooling from* 280 °C *to room temperature*): According to the ultrasonic and AE results, this stage is probably characteristic of a slower development of the damage process than for the previous temperature domain. In fact, a slight deceleration of the Young's modulus fall is associated to a notable inflection of R_T.

Period I (*heating from room temperature to* 870 °C): Back to room temperature, the sample is significantly damaged (Fig. 1) because of the thermal cycle. The low value of the Young's modulus ($E \approx 17$ GPa) is characteristic of a poor cohesion between the grains and the matrix. When temperature rises, an expansion of the material is quoted on the dilatometric curve (Fig. 10). According to our model (Fig. 11), the size of the grains, having a stronger dilation, approaches that of their cavity and few contacts appear at the interface and generate bursts of acoustic emission. A slight increase in the Young's modulus evolution coupled to a notable rise of the acoustic emission activity ($R_T = 0.18\,K^{-1}$) is observed. This can be attributed to the beginning of consolidation process within the material. At this step of the discussion, it is interesting to focus on the slope of the dilatometric curve obtained for periods IV and V and the one issued from period I (Fig. 10). It is clear that the CTE measured during the heating stage (period I) is higher than the one noted at the end of the cooling stage (periods IV and V). This lack of symmetry in the behaviour can be explained by a hysteretic effect most probably due to interfacial displacement occurring between grain surfaces. Indeed, one can easily imagine that, at the beginning of the heating stage, the relative free location of the mullite grains in their cavity induces a placement of these grains not rigorously equivalent to that which they occupied at room temperature. Early contacts at the interface occur (recorded in EA) which make the CTE of the material increasing.

Period II (*heating from* 870 *to* 1215 °C): In this temperature domain, the sudden increase of E modulus associated with

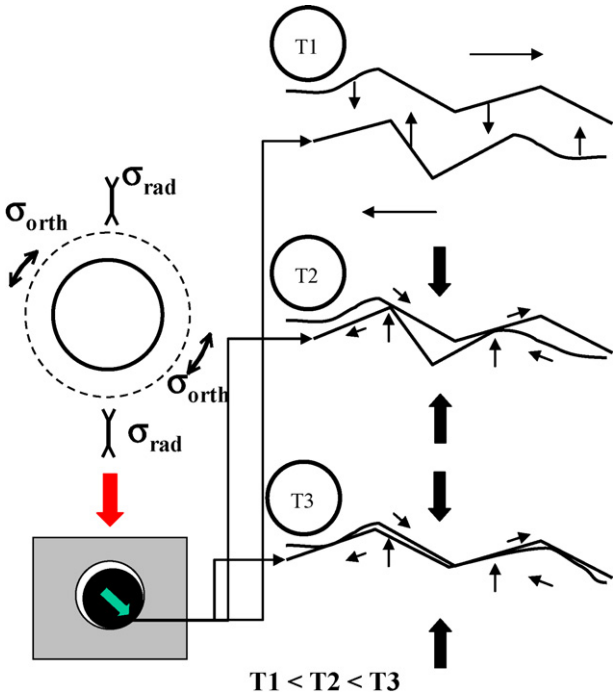

Fig. 11. Schematic representation of residual stresses developed and hypothesis on mechanisms acting during the heating stage: (T1) expansion and bringing together of the free surfaces of the crack; (T2) first contacts and slight frictions; and (T3) established contacts and frictions.

a higher AE hit rate ($R_T = 0.5\,K^{-1}$) are most probably closely related to significant friction mechanisms occurring between the free surfaces of the open cracks (very close at this time). From that point, the grain starts to occupy the entire place which is intended to it (Fig. 11). The interface is reconstituted and is then solicited under coupled compression-shear stresses. The Young's modulus has more than doubled ($E \approx 40$ GPa). The healing process of the cracks has also started at the end of this stage. Indeed, at high temperature, a low viscosity vitreous phase comes to partially fill the interstices. The occurring of this phase is the origin of the attenuation of the ultrasonic waves quoted in US echography.

5. Conclusion

In industrial applications, the cycles of production, in which cordierite–mullite refractories are involved, impose daily thermal repeated alternations to them. These conditions of thermal fatigue cause early ageing, sometimes prejudicial to the behaviour in service of these materials.

On the sights of the experimental results, several observations can be done:

Firstly, a similarity in the number of distinct temperature domains (5) and their relative extend is observed between the Young's modulus evolution and the AE activity variation both vs. temperature. This shows the good correlation obtained between the results of the two ultrasonic methods supported by dilatometry measurements.

Secondly, an acoustic emission activity is not only present during the cooling phase, but also during the heating one. Of

course, the hit rates R_T (Table 2) are not of the same order of magnitude (100 times lower for the heating stages compared to the cooling ones), but the number of recorded signals is significant to underline the sensitivity of this technique to phenomena which are not exclusively related to a microstructural change or a damage process.

Thirdly, a consolidation of the material during the heating stage and a notable fall of rigidity, for a given temperature domain, during the cooling period are emphasised. A hysteretic effect on the Young's modulus variation is also underlined. Indeed, because of their coarse grains, heterogeneous and multiscale structure, refractory materials can exhibit such behaviours. Some research works report a hysteretic loop shape for Young's modulus variations vs. temperature. For example, Case et al.[23] have observed hysteretic phenomena on anisotropic coarse grained alumina material and Nonnet et al.[24] so as Baudson et al.[9] have underlined similar behaviours for alumina castables and MgO/C refractories. These effects are not always due to the same physical mechanisms. However, most frequently, they can be explained by the thermal expansion mismatch between the solid phases.

The thermal expansion mismatch between the mullite grains and the matrix of cordierite inevitably generates the formation of a microcracks and decoherences network during cooling. Other results not presented here show that this damage affects the mechanical properties (failure stress at room temperature). This effect increases with the number of thermal cycles applied to the material (even for relatively low maximum temperatures). When the maximum temperature is sufficiently high, the low viscosity vitreous phase present in the material allows a "transitory" healing process of this damage and induces a restoration of the mechanical properties.

In the low temperatures domain, by reducing at the same time the elastic properties and the CTE, the damage process improves most probably the resistance to thermal shocks of these materials.

This work is part of a wider study aiming to understand the thermomechanical behaviour of these materials. The combined use of two non-destructive characterisation techniques, AE and US Echo respectively, associated with dilatometry measurements, made it possible to better understand the phenomena acting during the imposed thermal cycle.

Acknowledgment

The authors would like to thank the referees for their helpful remarks.

References

1. Ibrahim, D. M., Naga, S. M., Abdel Kader, Z. and Abdel Salam, E., Cordierite–mullite refractories. *Ceram. Int.*, 1995, **21**, 265–269.
2. Boccaccini, D. N., Leonelli, C., Rivasi, M. R., Romagnoli, M. and Boccaccini, A. R., Microstructural investigations in cordierite–mullite refractories. *Ceram. Int.*, 2005, **31**, 417–432.
3. Chen, H. L., Cheng, C. T. and Chen, S. E., Determination of fracture parameters of mortar and concrete beams by using acoustic emission. *Mater. Eval.*, 1992, 888–894.
4. Prosser, W. H., Jackson, K. E., Kellas, S., Smith, B. T., McKeon, J. and Friedman, A., Advanced waveform-based acoustic emission detection of matrix cracking in composites. *Mater. Eval.*, 1995, 1052–1058.
5. Berkovits, A. and Fang, D., Study of fatigue crack characteristics by acoustic emission. *Eng. Fract. Mech.*, 1995, **51**, 401–416.
6. Barré, S. and Benzeggagh, M. L., On the use of acoustic emission to investigate damage mechanisms in glass–fibre-reinforced polypropylene. *Comp. Sci. Technol.*, 1994, **52**, 369–376.
7. Chotard, T., Smith, A., Rotureau, D., Fargeot, D. and Gault, C., Acoustic emission characterisation of calcium aluminate cement hydration at an early stage. *J. Eur. Ceram. Soc.*, 2003, **23**, 387–398.
8. Chotard, T., Quet, A., Ersen, A. and Smith, A., Application of the acoustic emission technique to characterise liquid transfer in a porous ceramic during drying. *J. Eur. Ceram. Soc.*, 2006, **26**, 1075–1084.
9. Baudson, H., Debucquoy, F., Huger, M., Gault, C. and Rigaud, M., Ultrasonic measurement of Young's modulus MgO/C refractories at high temperature. *J. Eur. Ceram. Soc.*, 1999, **19**, 1895–1901.
10. Huger, M., Fargeot, D. and Gault, C., High temperature measurement of ultrasonic wave velocity in refractory materials. *High Temp.-High Press.*, 2002, **34**, 193–201.
11. Bakuckas, J. G., Prosser, W. H. and Johnson, W. S., Monitoring damage growth in titanium matrix composites using acoustic emission. *J. Comp. Mater.*, 1994, **28**, 305–328.
12. Suzuki, H., Takemoto, M. and Ono, K., The fracture dynamics in a dissipative glass fibber/epoxy model composite with AE source simulation analysis. *J. Acous. Emis.*, 1996, **14**, 35–50.
13. Pauchard, V., Brochado, S., Chateauminois, A., Campion, H. and Grosjean, F., Measurement of sub-critical crack-growth rates in glass fibbers by means of acoustic emission. *J. Mater. Sci. Lett.*, 2000, **19**, 2141–2143.
14. Havlicek, F. and Crha, J., Acoustic emission monitoring during solidification processes. *J. Acous. Emis.*, 1999, **17**, 3–4.
15. Coddet, C., de Barros, G. and Beranger, G., Influence of thermal cycling between 20 and 400 °C on the oxidation of copper. In *Proceedings of the European Symposium*, 1981, pp. 417–426.
16. Coddet, C., Chretien, J. F. and Beranger, G., Investigation on the fracture mechanism of oxide layers growing on titanium by acoustic emission. *Titan. Alloys Sci. Technol. Aspects*, 1982, **2**, 1097–1105.
17. Hamstad, M. A., Thompson, P. M. and Young, R. D., Flaw growth in alumina studied by acoustic emission. *J. Acous. Emis.*, 1987, **6**, 93–97.
18. Krietsch, T. and Bohse, J., Selection of acoustic emissions and classification of damage mechanisms in fibber composite materials. Progress in Acoustic emission XI, The Jap. Soc. For NDI, 1998, pp. 80–87.
19. Ono, K. and Huang, Q., Pattern recognition analysis of acoustic emission signals. Progress in Acoustic Emission VII, The Jap. Soc. For NDI, 1994, pp. 69–78.
20. Yuyama, S., Okamoto, T., Shigeishi, M. and Ohtsu, M., Quantitative evaluation and visualisation of cracking process in reinforced concrete by a moment tensor analysis of acoustic emission. *Mater. Eval.*, 1995 (June), 751–756.
21. Ohtsu, M., Okamoto, T. and Yuyama, S., Moment tensor analysis of acoustic emission for cracking process concrete. *ACI Struct. J.*, 1998 (March–April), 87–95.
22. Wu, K., Chen, B. and Yao, W., Study on the AE characteristics of fracture process of mortar, concrete and steel–fibre-reinforced concrete beams. *Cem. Conc. Res.*, 2000, **30**, 1495–1500.
23. Case, E. D., Smyth, J. R. and Hunter, O., Microcracking in large-grain Al_2O_3. *Mater. Sci. Eng.*, 1981, **51**, 175–179.
24. Nonnet, E., Lequeux, N. and Boch, P., Elastic properties of high alumina cement castables from room temperature to 1600 °C. *J. Eur. Ceram. Soc.*, 1999, **19**, 1575–1583.